



Thermodynamic and Economic Analysis of a Novel Solar-Assisted Ground Source Absorption Heat Pump System

Qingxuan Sun¹; Zachary E. Lee²; Zhiping Li³; K. Max Zhang⁴; Peijun Yang⁵; and Jiangfeng Wang⁶

Abstract: Hybrid utilization of solar and geothermal energy is an attractive option to solve the global energy crisis as well as environmental issues. A solar-assisted ground source absorption heat pump (SGSAHP) system is proposed to provide a solution to energy shortage, especially in remote regions without reliable electricity supply. The SGSAHP system requires little electricity input and is able to maximize the use of renewable energy and minimize the peak demand to the power system. The system exploits solar and geothermal energy, which can improve the coefficient of performance (COP) of the system and make it operate with little electricity input. SGSAHP can run under both heating mode and cooling mode. In this paper, a SGSAHP mathematical model is developed and simulation study is conducted including parameter analysis, economic analysis, and system optimization. The results show that there exists an optimal value of the generator temperature to reach the maximum COP, while higher condenser temperature and evaporator temperature have negative and positive influence on system performance, respectively. The optimized thermodynamic and economic performance is obtained. The exergy analysis shows that the major exergy losses are contributed by solar collector and heat exchanger. DOI: 10.1061/(ASCE)EY.1943-7897.0000747. © 2021 American Society of Civil Engineers.

Author keywords: Absorption heat pump; NH₃-H₂O; Solar; Geothermal; Heating and cooling.

Introduction

With the development of technology and the expansion of cities, worldwide energy consumption is rapidly increasing. A large portion of this increase can be attributed to building climate control (IEA 2017). Currently, buildings are cooled by air conditioning and are heated directly with either fossil fuels or electricity. However, recent advances in heat pump technology have allowed heat pumps to be an efficient alternative to conventional heating and cooling for a number of scenarios (Chua et al. 2010). However, heat pumps are usually driven by grid electricity, which is not necessarily generated from clean sources. Furthermore, a wide adoption of electricity-driven heat pumps for heating and cooling will exacerbate the peak demand problem, which has enormous economic and environmental consequences. For example, during summer peak periods, huge problems of grid reliability and public

health can be caused by air conditioning usage, high electricity prices, high temperatures, and high air pollution levels (Zhang and Zhang 2015). In addition, electricity-driven heating using heat pumps will likely create new wintertime peak demand challenges. Therefore, it is crucial to identify building climate control solutions that maximize the use of renewable energy and minimize the peak demand.

One potential solution is to use on-site renewable electricity, e.g., from solar and wind, to power heat pumps directly. Because the electricity is directly provided by on-site generation, the renewables-powered heat pump systems have less influence on the peak demand of the power grid. However, energy storage is usually necessary to ensure reliability, which in turn increases the cost of the systems. Hawlader et al. (2001) studied a solar-assisted heat pump and conducted an experiment to analyze the heat pump performance. The solar-assisted heat pump could obtain a coefficient of performance (COP) of 4–9 in Singapore. A direct-expansion solar-assisted heat pump (DX-SAHP) system was experimentally studied to verify its performance under different weather conditions (Kuang and Wang 2006). The DX-SAHP could be operated under a daily-average COP of 2.6–3.3. Ji et al. (2008) studied a photovoltaic solar-assisted heat pump (PV-SAHP) system and analyzed the dynamic performance. The result showed that this heat pump system could reach a COP of 10.4 and a PV efficiency of 13.4%. Bellos and Tzivanidis (2019) proposed a solar-assisted heat pump combined with photovoltaic. The compressor is driven using PV electricity while solar-heated water can heat the working fluid in the evaporator. In Braimakis et al. (2017), a heat pump powered by photovoltaic panels was proposed and compared with an organic Rankine cycle trigeneration system. The result showed that the heat pump system had an efficiency of 15% and a payback period (PP) of 12.1 years. Thygesen and Karlsson (2014) studied and compared the economics of various heat pumps with battery or water

¹Ph.D. Candidate, School of Energy and Power Engineering, Xi'an Jiaotong Univ., Xi'an 710049, People's Republic of China.

²Ph.D. Candidate, Sibley School of Mechanical and Aerospace Engineering, Cornell Univ., Ithaca, NY 14853.

³Director, Shannxi HanWang Pharmaceutical Co., Ltd., Yingbin West Rd., Hanzhong, Shaanxi Province 723000, People's Republic of China.

⁴Professor, Sibley School of Mechanical and Aerospace Engineering, Cornell Univ., Ithaca, NY 14853.

⁵Director, Xi'an Thermal Power Research Institute Co., Ltd., Yanxiang Rd., Xi'an, Shaanxi Province 710054, People's Republic of China.

⁶Professor, School of Energy and Power Engineering, Xi'an Jiaotong Univ., Xi'an 710049, People's Republic of China (corresponding author). Email: jfwang@xjtu.edu.cn

Note. This manuscript was submitted on March 24, 2020; approved on November 23, 2020; published online on February 5, 2021. Discussion period open until July 5, 2021; separate discussions must be submitted for individual papers. This paper is part of the *Journal of Energy Engineering*, © ASCE, ISSN 0733-9402.

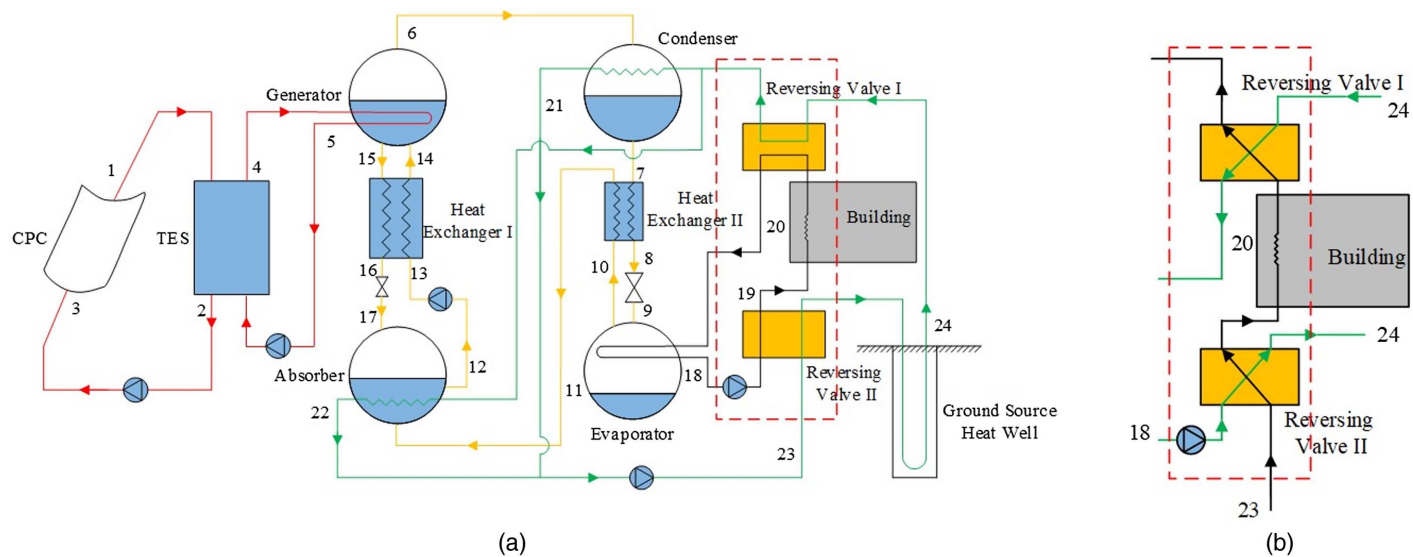


Fig. 1. Solar-assisted ground source absorption heat pump: (a) cooling mode; and (b) heating mode.

storage tank. They found that the cost of electricity of battery storage is two times higher than the cost of hot water storage. Mazzeo (2019) studied an electric vehicle charging station trigeneration heat pump system assisted by solar and wind energy to meet the cooling, heating, and electric demand. In this study, wind and photovoltaic generators generate electricity to power heat pumps and electrical demand, while excess energy is stored in batteries. Extensive research has been conducted on the renewables-powered heat pump recently (Song et al. 2019; Wu et al. 2019; Zheng et al. 2016a).

Another potential solution is solar-assisted ground source heat pumps (GSHPs), which utilize solar thermal energy to improve system COP, even though electricity input is still required. Ozgener and Hepbasli (2005) conducted an experimental solar-assisted GSHP for heating and demonstrated overall high efficiency for this application. Ozgener (2010) proposed a solar-assisted GSHP combined with wind turbine system for heating. Their simulation result indicated that the combined system could be economically preferable to conventional systems for building heating. Zheng et al. (2016b) proposed a solar and ground source heat pump coupling system and developed a new type of heat storage. The experimental result showed that the COP can be 6.96. Únal et al. (2018) conducted energy, exergy, and exergoeconomic (3E) analysis on a solar-assisted GSHP system operating in heating seasons.

The solution that we focus on in this paper is renewable-assisted absorption heat pump. Different from other heat pumps that primarily rely on external electricity sources (mainly to power the compressors in the vapor compression refrigeration cycles), the absorption heat pump needs very little electricity input because it is driven by the fluid concentration and temperature differences. Absorption heat pumps based on renewable energy like solar energy or geothermal energy have attracted some attention. Wu et al. (2014a) gave a review of recent developments and technologies of absorption heat pumps and their applications in industry. Wu et al. (2016) presented a water source $\text{NH}_3\text{-H}_2\text{O}$ absorption heat pump for heating that can reach a high COP with heat source temperatures from 110°C to 140°C , and the evaporator inlet temperature can reach 18°C . Jia and Dai (2018) investigated an $\text{NH}_3\text{-H}_2\text{O}$ absorption-resorption heat pump cycle for heating. The system can be operated under the ambient temperature of 7.5°C or higher and the heat

source temperature of 85°C . Hernández-Magallanes et al. (2018) analyzed a system combining heat pump with a turbine to produce heat and power simultaneously.

However, while solar-assisted and geothermal-assisted absorption heat pumps have been investigated independently, there is little research on integrating both solar and geothermal energy with absorption heat pumps. Moreover, in terms of performance evaluations, most previous studies for absorption heat pump focus on heating-only or cooling-only applications, and few have analyzed the performance for both heating and cooling. In this work, a novel solar-assisted ground source absorption heat pump (SGSAHP) is proposed to efficiently use renewable resources for producing heating and cooling energy while greatly reducing the electricity consumption and thus the contribution to the peak demand problem. Moreover, due to the low electricity input, it can also be applied in regions with unreliable electricity to improve the power grid services and living standards. In this system, thermal energy storage (TES) is introduced to allow continuous operation. The mathematical model is introduced, and thermodynamic and economic analyses are conducted to examine the effects of key parameters. Optimization is also conducted by using genetic algorithms (GAs) to obtain optimal system performance.

System Description

Fig. 1 is the schematic diagram of the SGSAHP system. The system has two working modes: cooling mode running in summer and heating mode running in winter. As shown in Fig. 1(a), the system running in cooling mode consists of four subcycles: solar cycle (1–5); absorption heat pump cycle (6–17); building cycle (18–20); and geothermal cycle (21–24).

In the traditional absorption heat pump cycles, the working fluid is heated by an electrical heater in the generator. However, the addition of a solar collector can supply this heat, eliminating the need for electrical input. The ground source heat has the properties of stabilized temperature, which is lower than air. The combination of the three systems can significantly improve the absorption heat pump system performance.

The SGSAHP can run in cooling and heating mode (Fig. 1) by using a reversing valve. In cooling mode, the solar energy is

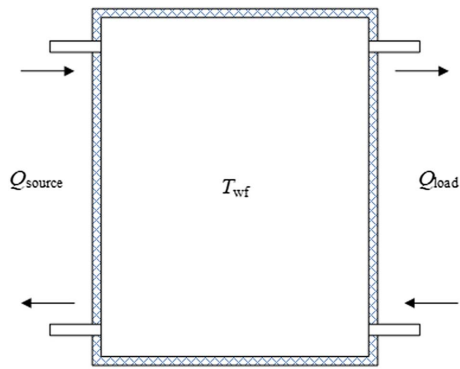


Fig. 2. Structure of thermal energy storage.

collected by a compound parabolic collector (CPC) and stored in TES using water. The working fluid in the absorption heat pump cycle is a mixture of ammonia (refrigerant) and water (absorbent). The $\text{NH}_3\text{-H}_2\text{O}$ working fluid becomes highly purified ammonia vapor (6) by absorbing the solar energy in the generator. The high-temperature ammonia vapor is then condensed by water from the ground source heat well to a saturated liquid (7). After expanding in the valve (9), the ammonia liquid extracts cold energy to the building in the evaporator and becomes vapor (10). Then the ammonia vapor is absorbed to a high-concentration ammonia solution (12) with a low-concentration ammonia solution (17) in the absorber by the water from the ground source heat well. The solution is sent to the generator to be separated into ammonia vapor (6) and low-concentration ammonia solution (15). The two heat exchangers in the system can improve system efficiency. By switching the reversing valves, the system can run in heating mode. The operation parameters are the same as running in cooling mode. The differences are that heat energy is extracted from ammonia refrigerant in the condenser and absorber and cold energy is supplied by the ground source heat well.

In this study, the SGSAHP system is studied from the perspective of simulation. First, the system models based on thermodynamics and exergy are built. Second, parameter-sensitive analysis is conducted to measure the effects of important parameters on system performance. Third, system daily performance and economic analysis are conducted with a time step of 1 h. At last, the system is optimized by using genetic algorithm.

Mathematical Model

To conduct the thermodynamic analysis of SGSAHP, some assumptions are made:

1. The steady-state refrigerant is 99.9% $\text{NH}_3\text{-H}_2\text{O}$;
2. Pressure changes are neglected except in valves and pumps;
3. There is only saturated liquid at Points 7, 12, and 15;
4. There is only saturated vapor at Point 6;
5. Pumps have a given isentropic efficiency; and
6. All the energy generated by SGSAHP will be consumed by the building.

Solar Collector and Thermal Energy Storage

Compound parabolic collectors are selected to collect energy for the solar collector subsystem. The CPC absorbed solar radiation flux can be expressed as

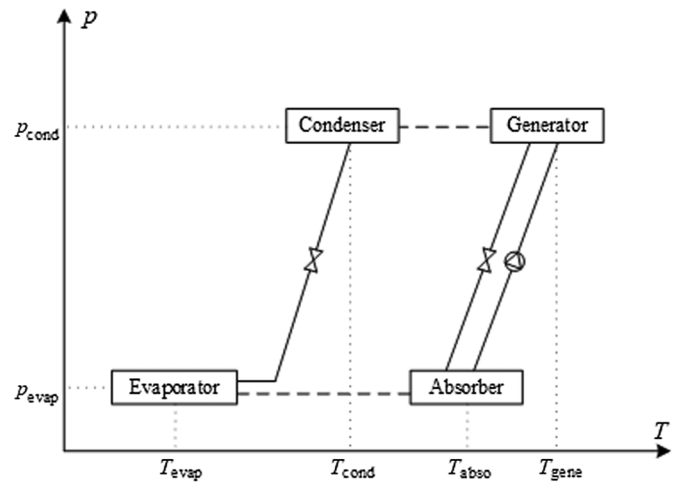


Fig. 3. p - T diagram of absorption heat pump cycle.

$$S = \left[I_{\text{bm}} R_{\text{bm}} + \frac{I_{\text{dif}}}{C} \right] \tau \rho \alpha \quad (1)$$

Due to CPC's large acceptance angle, beam and diffuse solar radiation can be absorbed. The subscripts bm and dif in Eq. (1) represent the absorbed beam and diffuse radiation, respectively.

The heat gain rate Q_{solar} is described as

$$Q_{\text{solar}} = F_R W L \left[S - \frac{U_{\text{lo}}}{C} (T_{\text{stg}} - T_{\text{amb}}) \right] \quad (2)$$

In this study, an insulated water thermal energy storage is introduced between the solar collector and the absorption heat pump cycle. The structure of TES can be seen in Fig. 2. To simplify the calculation, we assume that the thermal energy storage is a single-volume heat storage tank, the internal working fluids are fully mixed, and the temperature is evenly distributed. Energy balance in TES is shown as (Sukhatme 1984)

$$[(\rho V c_p)_w + (\rho V c_p)_t] \frac{dT_{\text{stg}}}{dt} = Q_{\text{solar}} - Q_{\text{load}} - UA(T_{\text{stg}} - T_{\text{amb}}) \quad (3)$$

where $(\rho V c_p)_w$ and $(\rho V c_p)_t$ = heat capacities of the water in the tank and the tank material, respectively.

Absorption Heat Pump

The p - T diagram of the $\text{NH}_3\text{-H}_2\text{O}$ absorption heat pump cycle is shown as Fig. 3. The condenser and generator are working at the same high pressure, while the evaporator and absorber operate at the same low pressure. The pressure is controlled by valves and a pump. The system performance can be obtained based on governing equations of each component

$$\sum \dot{m}_{\text{in}} = \sum \dot{m}_{\text{out}} \quad (4)$$

$$\sum \dot{m}_{\text{in}} x_{\text{in}} = \sum \dot{m}_{\text{out}} x_{\text{out}} \quad (5)$$

$$Q + \sum \dot{m}_{\text{in}} h_{\text{in}} = \sum \dot{m}_{\text{out}} h_{\text{out}} \quad (6)$$

The system model based on each component is listed as follows.

In the evaporator, the heat gained from the building is calculated by

$$Q_{\text{evap}} = \dot{m}_{10}h_{10} - \dot{m}_9h_9 = \dot{m}_{\text{ref}}(h_{10} - h_9) \quad (7)$$

The NH₃-H₂O vapor generated in the evaporator is absorbed in the absorber. Energy consumption in the absorber is calculated as

$$Q_{\text{abso}} = \dot{m}_{12}h_{12} - \dot{m}_{11}h_{11} - \dot{m}_{17}h_{17} \quad (8)$$

The NH₃-H₂O working fluid absorbs energy in the generator. The energy balance in the generator is

$$Q_{\text{gene}} = \dot{m}_6h_6 + \dot{m}_{15}h_{15} - \dot{m}_{14}h_{14} \quad (9)$$

The generated vapor discharge heat to water from the ground source heat well in the condenser is

$$Q_{\text{cond}} = \dot{m}_6h_6 - \dot{m}_7h_7 = \dot{m}_{\text{ref}}(h_6 - h_7) \quad (10)$$

The heat transferred in the heat exchangers can be calculated as

$$\begin{aligned} Q_{\text{HEX I}} &= \dot{m}_{15}h_{15} - \dot{m}_{16}h_{16} = \dot{m}_{14}h_{14} - \dot{m}_{13}h_{13} \\ &= \dot{m}_{\text{ics}}(h_{15} - h_{16}) = \dot{m}_{\text{hcs}}(h_{14} - h_{13}) \end{aligned} \quad (11)$$

$$Q_{\text{HEX II}} = \dot{m}_7h_7 - \dot{m}_8h_8 = \dot{m}_{11}h_{11} - \dot{m}_{10}h_{10} = \dot{m}_{\text{ref}}(h_7 - h_8) \quad (12)$$

The pump power consumption is given by

$$W_{\text{pump}} = \dot{m}_{\text{hcs}}(h_{13} - h_{12})/\eta_{\text{pump}} \quad (13)$$

The mass balances in the generator and absorber are

$$\dot{m}_6 + \dot{m}_{15} = \dot{m}_{14} \quad (14)$$

$$\dot{m}_{11} + \dot{m}_{17} = \dot{m}_{12} \quad (15)$$

$$\dot{m}_6x_6 + \dot{m}_{15}x_{15} = \dot{m}_{14}x_{14} \quad (16)$$

$$\dot{m}_{11}x_{11} + \dot{m}_{17}x_{17} = \dot{m}_{12}x_{12} \quad (17)$$

These equations can be summarized as

$$\dot{m}_{\text{ref}} + \dot{m}_{\text{ics}} = \dot{m}_{\text{hcs}} \quad (18)$$

$$\dot{m}_{\text{ref}}x_{\text{ref}} + \dot{m}_{\text{ics}}x_{\text{ics}} = \dot{m}_{\text{hcs}}x_{\text{hcs}} \quad (19)$$

Exergy Model

For a steady system, it is important to analyze exergy of the system to measure the energy utilization performance.

For a point i in the system, the exergy can be defined as

$$E_i = \dot{m}_i[(h_i - h_a) - T_a(s_i - s_a)] \quad (20)$$

For a single unit, the exergy balance is (Lior and Zhang 2007)

$$\sum E_{\text{input}} - \sum E_{\text{output}} = I \quad (21)$$

For the ground source heat exchanger, the exergy loss can be calculated by the exergy balance

$$I_{\text{gh}} = \dot{m}_{\text{ground-water}}(E_{24} - E_{23}) + Q_{\text{gh}} \left(1 - \frac{T_{\text{amb}}}{T_{\text{soil}}}\right) \quad (22)$$

where Q_{gh} = energy gained from ground source heat described as

$$Q_{\text{gh}} = \dot{m}_{23}(h_{24} - h_{23}) \quad (23)$$

The system exergy loss can be expressed as

$$I_{\text{sys}} = \sum I \quad (24)$$

Performance Indexes Definition

In this section, several indexes of the system for performance evaluation are defined.

The heat and cold energies delivered to the building can be calculated respectively as

$$Q_{\text{building}} = Q_{\text{cond}} + Q_{\text{abso}} \quad (25)$$

$$Q_{\text{building}} = Q_{\text{evap}} \quad (26)$$

where Eq. (25) is heating mode energy in winter and Eq. (26) is the cold energy in summer.

The COP for absorption heat pump cycle is given as

$$\text{COP}_{\text{hp}} = \frac{Q_{\text{building}}}{Q_{\text{gene}} + Q_{\text{gh}} + P_{\text{pump}}} \quad (27)$$

The daily system exergy efficiency η_{exg} is calculated as

$$\eta_{\text{exg}} = \frac{\int Q_{\text{building}} \left[1 - \frac{T_{\text{amb}}}{T_{\text{building}}}\right]}{\int \left(P + Q_{\text{gh}} \left[1 - \frac{T_{\text{amb}}}{T_{\text{soil}}}\right] + Q_{\text{solar}} \left[1 - \frac{4}{3} \frac{T_{\text{amb}}}{T_{\text{solar}}} + \frac{1}{3} \left(\frac{T_{\text{amb}}}{T_{\text{solar}}}\right)^4\right] \right)} \quad (28)$$

where T_{solar} = solar radiation temperature (Banat and Jwaied 2008).

Economic Analysis

Economic analysis is an important method to evaluate the viability of implementing this design. In this economic analysis, we consider the solar collector, thermal energy storage, absorption heat pump, and geothermal well. The currency used in this study is the Chinese yuan.

First, the net present value (NPV) indicates the present value of a system investment. Therefore, NPV takes the future gains and discount into account so that it can reflect the true value of the system over time. NPV can be expressed as

$$\text{NPV} = -C_0 + \sum_{j=1}^M \frac{CF_{\text{net}}}{(1+r)^j} \quad (29)$$

where r = discount factor; and M = project life.

The capital investment is a sum of all construction costs, including the costs of the solar collector, thermal energy storage, absorption heat pump, and geothermal well. Other miscellaneous costs are considered to be included in these terms. The following equation describes the way to calculate capital investment:

$$C_0 = C_{\text{ahp}} + C_{\text{solar}} + C_{\text{stg}} + C_{\text{well}} \quad (30)$$

The data of each parameter are given in Table 1.

The yearly cash flow is described as the income of energy output to buildings minus the cost of operation and maintenance and electricity

Table 1. Parameters of system economic model

Parameter	Value or equation	Units	Reference
Solar collector cost	$1,960 \times A^{0.95}$	¥	Voros et al. (1998)
Thermal energy storage cost	$6,947 \times V$	¥	Voros et al. (1998)
Absorption heat pump cost	$2,084 \times Q_{\text{building}}$	¥	Mroz (2006), El-Gohary (2013)
Geothermal well cost	$11.86 \times 10^{-1} \times Z^2 + 15.87 \times 10^3 \times Z - 42.78 \times 10^5$	¥	Lukawski et al. (2014)
Operation and maintenance cost	0.1% capital investment	¥	Tsoutsos et al. (2003)
Discount factor	3%	—	—
Project life	25 years	—	—
Exchange rate	6.9	—	—

Note: Z = depth of the geothermal well.

Table 2. Constant parameters of the present study

Parameter	Value
City	Xi'an, China
Ambient temperature in summer (°C)	20
Ambient temperature in winter (°C)	5
Ambient pressure (MPa)	0.101
Cooling or heating load (kW)	10
Area of the aperture of CPC (m ²)	300
Concentration ratio of collector	6.50
Collector water mass flow rate (kg/s)	0.02
Solar radiation temperature (°C)	5,727
Ground source heat temperature in summer (°C)	15
Ground source heat temperature in winter (°C)	8
Pump efficiency (%)	65
Well depth (m)	350

Table 3. Variable parameters of the present study

Parameter	Symbol	Range
Generator temperature (°C)	T_{gene}	60–80
Evaporator temperature (°C)	T_{evap}	0–10
Condenser temperature (°C)	T_{cond}	25–35

$$CF_{\text{net}} = C_{\text{building}} - C_{\text{O\&M}} - C_e \quad (31)$$

Internal rate of return (IRR) is an indicator to show investment efficiency and can be expressed as

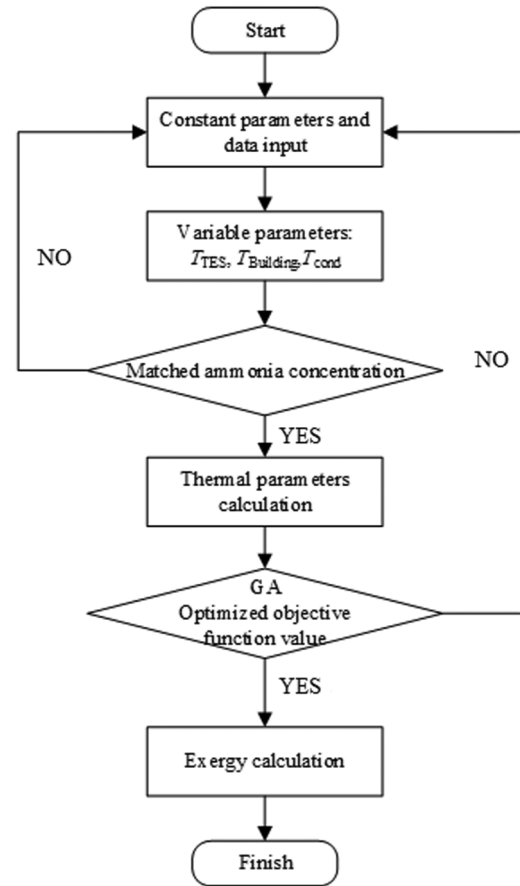
$$\text{IRR} = \frac{CF_{\text{net}}}{C_0} \left[1 - \frac{1}{(1 + \text{IRR})^M} \right] \quad (32)$$

The PP represents the time of investment to recover capital cost. The following equation shows the calculation of PP:

$$\text{PP} = \frac{\ln\left(\frac{CF_{\text{net}}}{CF_{\text{net}} - C_0 r}\right)}{\ln(1 + r)} \quad (33)$$

Simulation Setup

Xianyang, Shaanxi, China was chosen as a case city to conduct the simulation. April to September is considered the cooling season, and October to March is considered the heating season. January 1 and July 1 were chosen as typical dates to analyze the heating and cooling modes, respectively. MATLAB version 2019a was

**Fig. 4.** Simulation procedure.

the simulation environment and thermodynamic properties of all fluids were obtained from REFPROP version 9.0 (NIST 2013).

Table 2 includes all the fixed parameters in the present analysis, while Table 3 gives variable parameters. As some researchers (Wu et al. 2014b) have discussed, the soil temperature varies with time during the year. It will also be changed by the heat pump operation situation. However, the temperature varies little in a single day. Therefore, the ground source heat source temperatures, i.e., the soil temperatures, were set as a constant value in this work. Because the system works in both winter and summer with two corresponding operation modes, the heat sources of the condenser and evaporator are not the same in winter and summer. In summer, condenser temperature is determined by ground source heat temperature while evaporator temperature is determined by building temperature. The opposite is true in winter. For both seasons, the generator

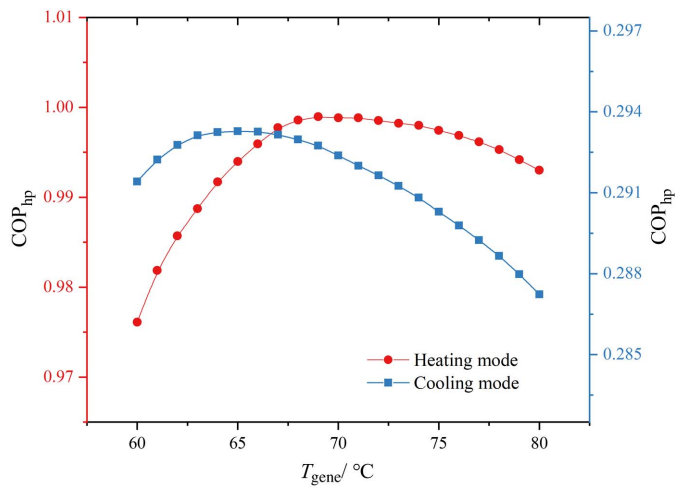


Fig. 5. Effects of generator temperature on system performance.

temperature in the absorption cycle is influenced by TES temperature. Fig. 4 is the flowchart of the simulation.

Results and Discussion

Parameters Sensitivity Analysis

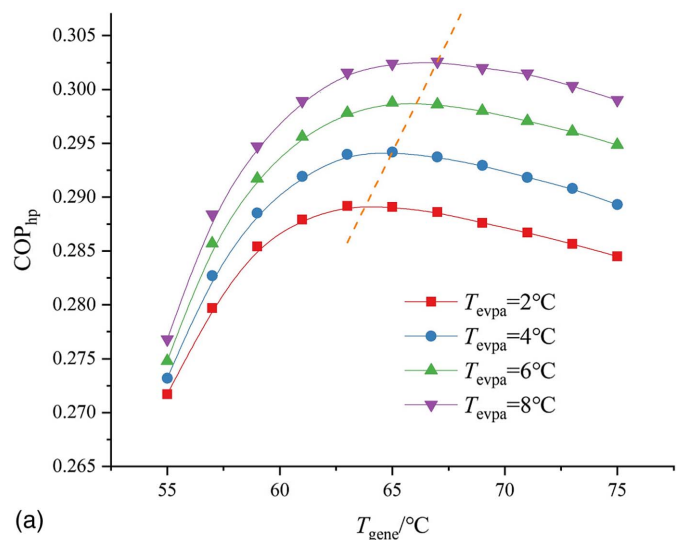
This subsection is devoted to exploring the influence of three key parameters on system performance: generator, condenser, and evaporator temperature. COP (COP_{hp}) and daily system exergy efficiency (η_{exg}) are evaluation indexes of system performance. The parameter influences on COP_{hp} are analyzed at first in order to obtain the influence on absorption heat pump cycle performance.

Fig. 5 illustrates the effect of the generator temperature on COP. With generator temperatures increasing, COPs of cooling and heating modes increase and are maximized for generator temperatures equal to 65°C and 70°C, respectively. As the generator temperature increases, the enthalpy of the ammonia water increases, leading to a higher system performance. However, when the generator temperature is too high, the increased irreversibility brings a negative effect on COP (Udayakumar 2008). The different optimal generator temperatures for cooling and heating modes are caused by the different working conditions and ambient values. In other words, there exist some optimal generator temperatures for heating and cooling modes to achieve the best thermodynamic performance.

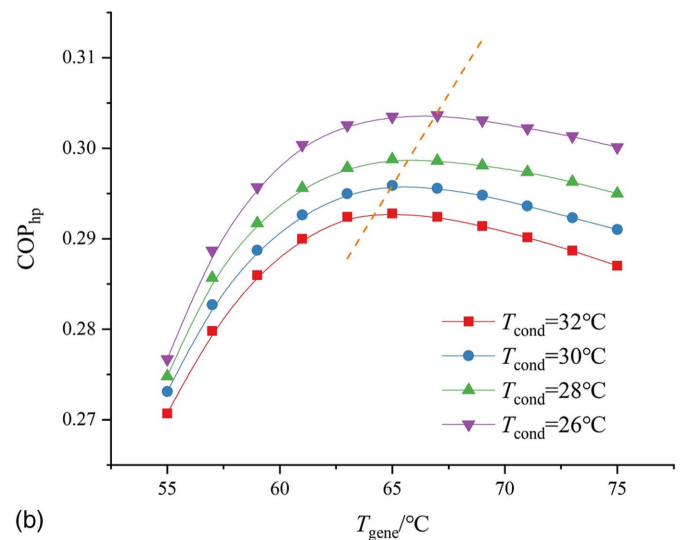
Cooling Mode Performance

Figs. 6(a–c) show the cooling mode performances for various generator, condenser, and evaporator temperatures. In each figure, two temperatures vary, while the other remains constant.

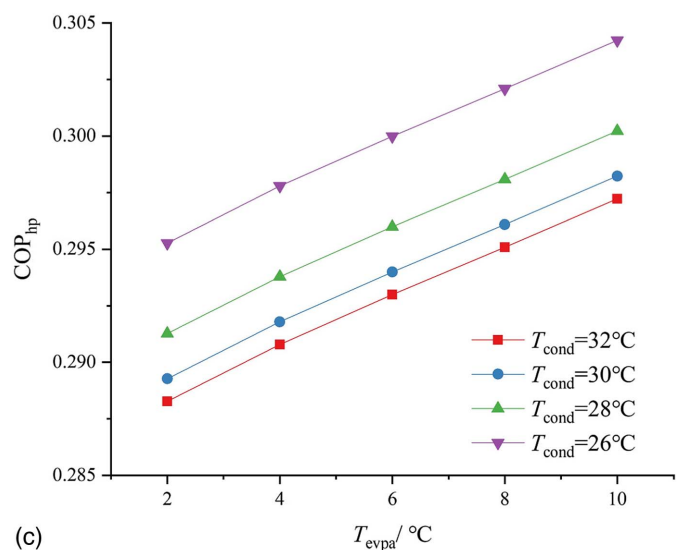
Fig. 6(a) illustrates the influences of generator and evaporator temperatures and Fig. 6(b) illustrates the influences of generator and condenser temperatures on cooling mode COPs. COPs increase with generator temperature increasing and are maximized with a generator temperature of 65°C. After this point, the COPs begin to decrease. This trend means that the generator temperature has an optimal value for system performance. The dashed lines in Figs. 6(a and b) show the best performance lines of evaporator and condenser temperatures separately. The influence of evaporator and condenser temperatures on cooling mode performance is illustrated in Fig. 6(c). The figures show that with evaporator



(a)



(b)



(c)

Fig. 6. Cooling mode performance for various temperatures: (a) generator and evaporator temperatures; (b) generator and condenser temperatures; and (c) condenser and evaporator temperatures.

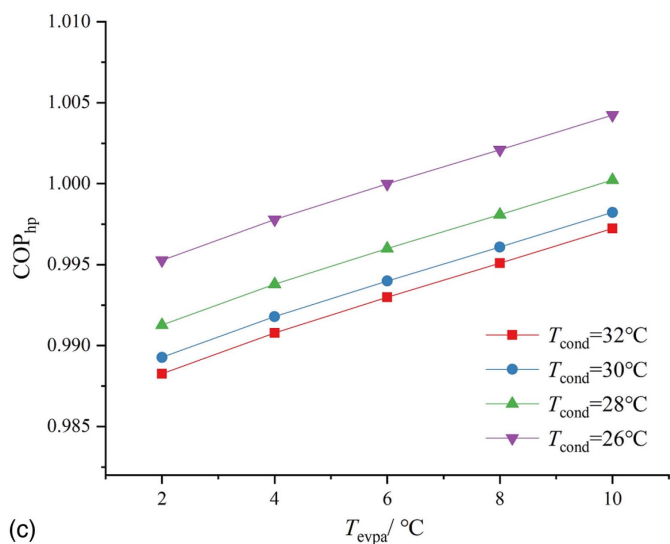
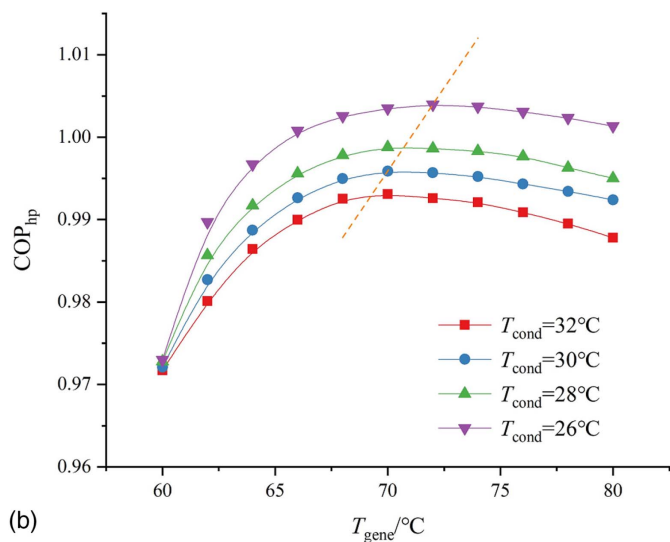
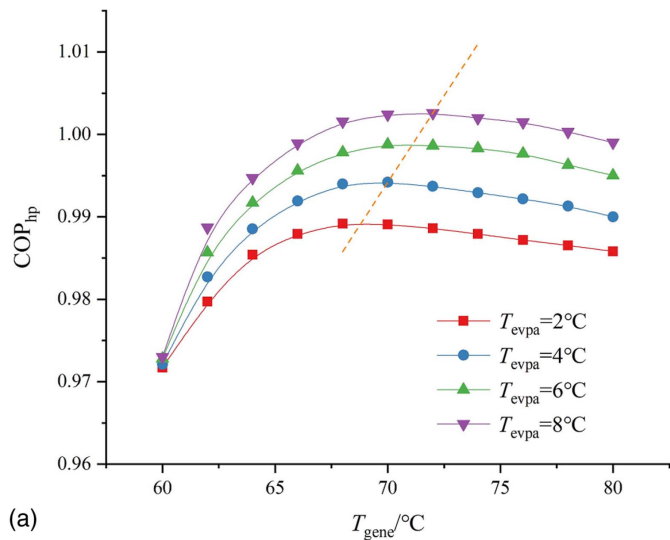


Fig. 7. Heating mode performance for various temperatures: (a) generator and evaporator temperatures; (b) generator and condenser temperatures; and (c) condenser and evaporator temperatures.

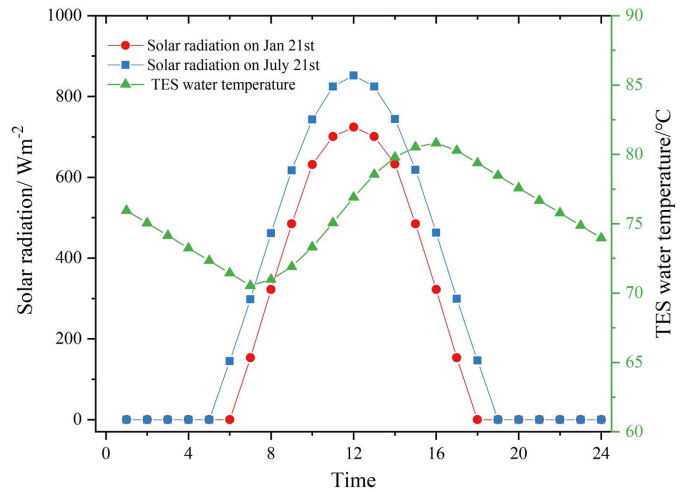


Fig. 8. Solar radiation comparison and TES temperature variation.

temperature increasing and condenser temperature decreasing, absorption heat pump performances become better.

Heating Mode Performance

Figs. 7(a-c) show the heating mode performances for various generator, condenser, and evaporator temperatures. Fig. 7(a) illustrates the effects of generator and evaporator temperatures and Fig. 7(b) illustrates the effects of generator and condenser temperatures on heating mode COPs. The trend is similar to the influence on cooling mode performance. All the curves in Figs. 7(a and b) have similar trends. For low generator temperatures, the COPs increase until it is maximized with a generator temperature around 70°C. After this point, the COPs begin to decrease. It means that the generator temperature has an optimal value for system performance. The dashed lines in Figs. 7(a and b) show the best performance lines of evaporator and condenser temperatures separately. Fig. 7(c) shows the influence of evaporator and condenser temperature on heating mode performance. It can be found that the system performance becomes better with the increase of evaporator and condenser temperatures.

In conclusion, in both cooling and heating modes, the higher evaporator temperature and lower condenser temperature bring a positive influence on system performance. The generator temperature has an optimal value for the best system performance.

Daily Performance

Fig. 8 shows the solar radiation on January 21 and July 21 and TES water temperature variation during a day. Due to the variation of the distance and angles from earth to the sun, the solar radiation varies every day. Fig. 8 shows that the hourly intensity and duration of solar radiation on July 21 is much higher than that on January 21. TES temperature has a fluctuation during a day. Solar radiation starts to increase when the sun rises. If the energy input to TES is more than energy output, the TES temperature increases. TES temperature decreases in the afternoon when TES input energy is less than output.

Fig. 9 shows the cooling and heating mode COPs with the variation of TES water temperature in a day. Generator temperature is decided by TES water temperature, so the variation of TES water temperature during a day significantly influences TES temperature and COPs. It can be seen that the cooling mode COPs increase at night and decrease during the day from 7:00 to 16:00. Due to the

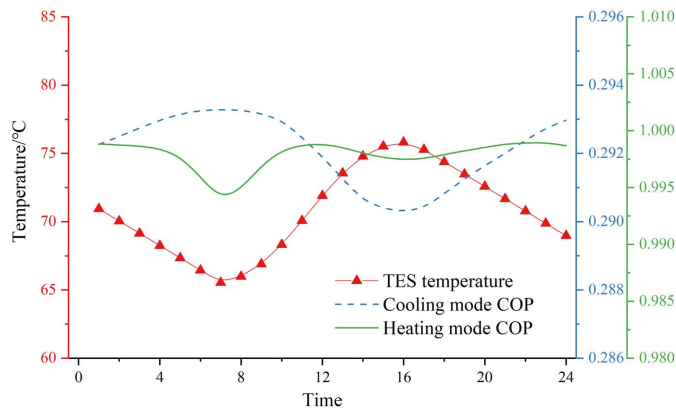


Fig. 9. Daily variation of generator temperature and heating and cooling mode COPs.

optimal generator temperature of the cooling mode of about 65°C, when the TES water temperature decreases at night, the COP increases and system performance improves. The system has the best performance at about 7:00 when the TES water temperature reaches about 65°C and has the worst performance at about 16:00 when the TES water temperature reaches the maximum value. The heating mode COP variation is complicated due to the optimal generator temperature of 70°C. The COP decreases twice in a day and reaches minimum values at around 7:00 and 16:00.

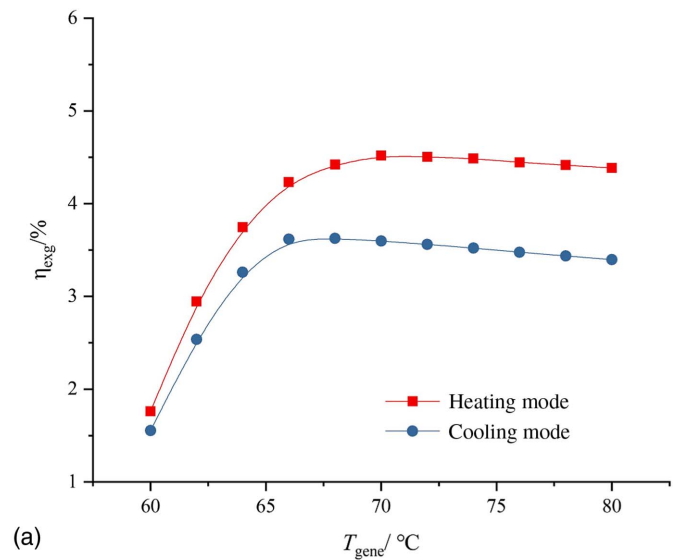
Figs. 10(a–c) show the influences of generator, evaporator, condenser temperatures on system exergy efficiency of heating and cooling modes. The figures show that a higher evaporator temperature has a positive influence on exergy efficiency, condenser temperature has a negative influence, and the generator has an optimal temperature to reach the best performance.

Economic Analysis

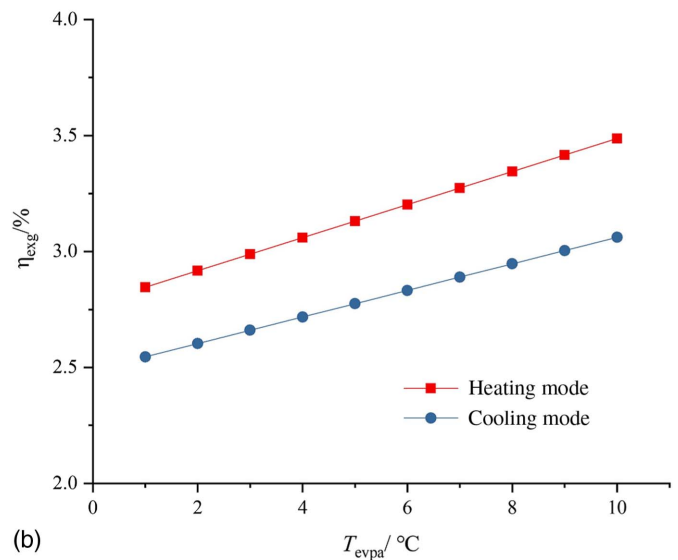
This subsection evaluates the economics of the system. The system cost is based on cooling mode because the system will be larger under cooling mode than heating mode due to the lower efficiency. The results are shown in Figs. 11(a–c).

The effects of generator temperature on economic performance are shown in Fig. 11(a). With the increase of generator temperature, the NPV increases, and the highest value can be 1.6 million yuan. However, the rate of increase is lower when the generator temperature is higher. The IRR increases at first and then decreases when the generator temperature is too high. With generator temperature increasing, payback period years decrease, leveling off at around 20 years, and energy output increase leads to higher NPV. However, the higher generator temperature also brings a higher capital investment, leading to a lower IRR. The effects of evaporator temperature on economic performance are illustrated in Fig. 11(b). With the increase of evaporator temperature, NPV and IRR increase and PP decreases, which positively influences economic performance. Fig. 11(c) exhibits the effects of condenser temperature on economic performance. The increasing condenser temperature has a negative influence on economic performance.

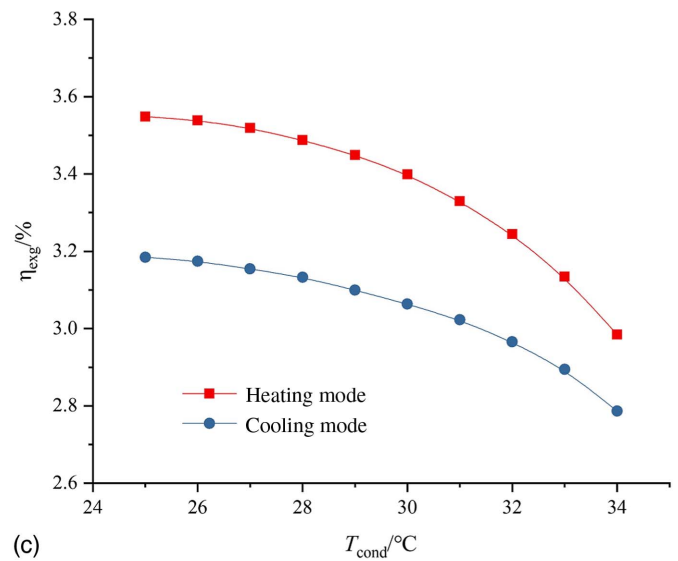
The economic result is a preliminary estimate for system design, performed by extrapolating the typical day results. However, the capital investment of the system is constant if the system had been designed, and the only changing part is operation cost and benefit. A typical day's economic result can reflect the economic performance relatively accurately. So the economic analysis method and result could be acceptable.



(a)



(b)



(c)

Fig. 10. Effects of temperature on daily exergy efficiency: (a) generator temperature; (b) evaporator temperature; and (c) condenser temperature.

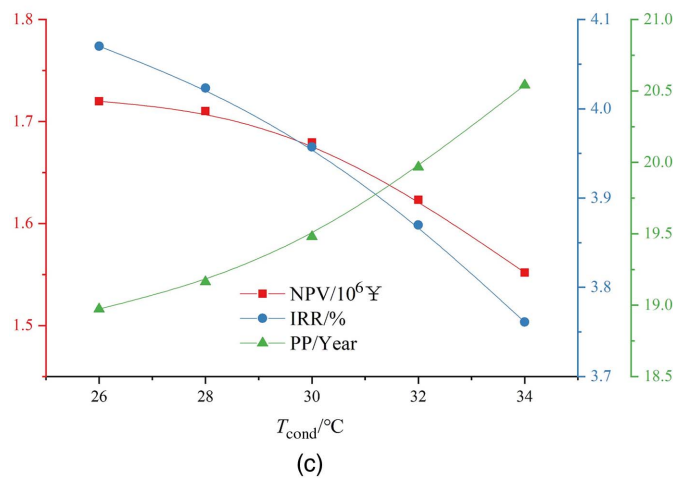
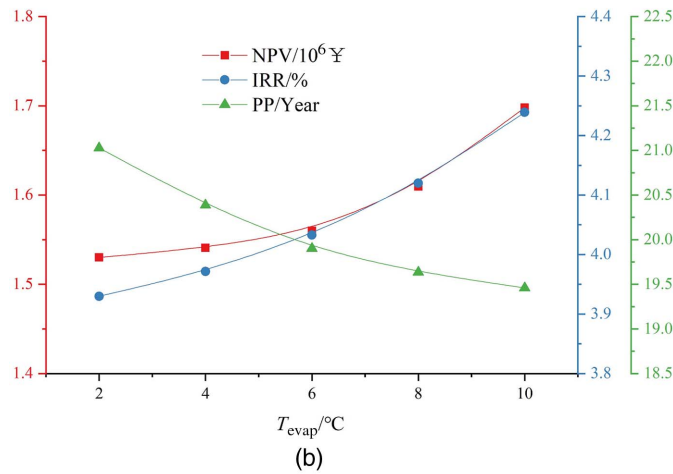
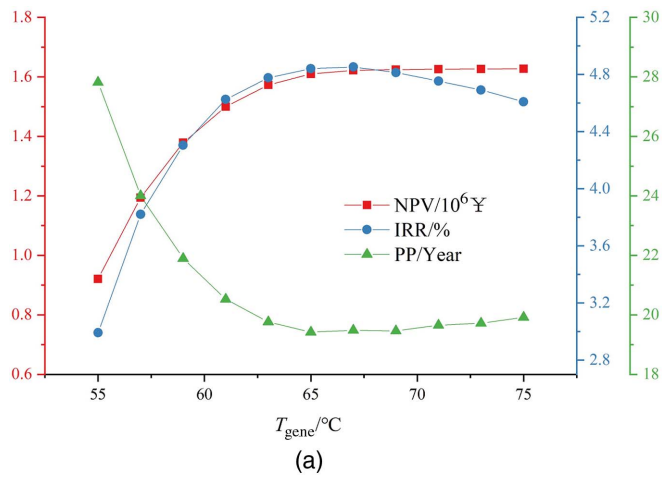


Fig. 11. Effects of parameters on economic performance: (a) generator temperature; (b) evaporator temperature; and (c) condenser temperature.

Optimization and Exergy Analysis

The previous analysis shows that the influences of three temperatures on system performance are different from each other. System optimization is necessary to conduct to find the optimized group of parameters to achieve the best performance. Hence, multiobjective optimization is conducted by using GA. Control parameters and the conditions of the genetic algorithm are given in Tables 4 and 5, respectively. For the same reason as previously, NPV and COP were chosen as objective functions based on cooling mode.

Table 4. Control parameters of GA

Control parameter	Value
Population size	90
Maximum generations	200
Crossover probability	0.8
Mutation probability	0.05
Selection process	Tournament

Table 5. Condition of the parameter optimization

Term	Lower limit	Upper limit
Generator temperature ($^{\circ}\text{C}$)	60	80
Evaporator temperature ($^{\circ}\text{C}$)	0	10
Condenser temperature ($^{\circ}\text{C}$)	25	35

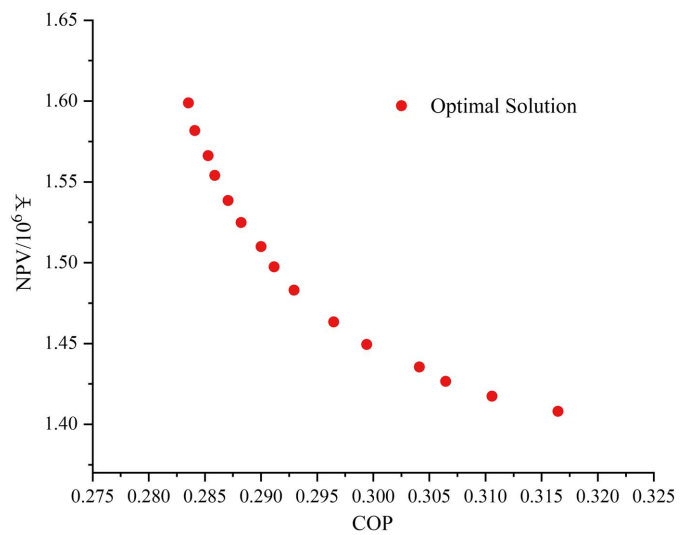


Fig. 12. Optimal solution for the COP versus the NPV.

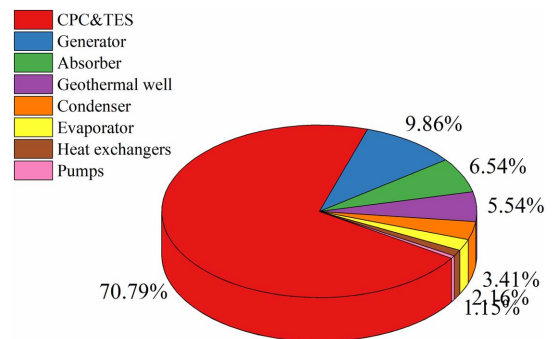


Fig. 13. Exergy loss distribution of cooling mode.

Fig. 12 illustrates the optimization result. With the increase of COP, NPV decreases. This means that we cannot reach high thermodynamic performance and economic performance simultaneously. Hence, an exergy analysis has been conducted and the result is illustrated in Fig. 13. From Fig. 13 we can see that the solar

collector and TES give the largest part of exergy losses because of the high solar radiation temperature and the huge temperature difference between the TES and generator. The generator and absorber also contribute a large part of exergy losses. The major exergy losses occur in heat exchangers due to the temperature difference. However, the temperature difference across the generator is much larger than the temperature difference across the absorber.

Conclusion

This paper proposed an SGSAHP that utilizes $\text{NH}_3\text{-H}_2\text{O}$ as the working fluid. Thermodynamic and economic analyses were conducted. Hybrid solar and geothermal energy were exploited in the absorption heat pump system, and both heating and cooling performance of the system were studied. The system will contribute to solving the peak demand problem and can be applied in remote regions with unreliable electricity to improve the power grid quality and living standards. The main conclusions are listed as follows:

- The SGSAHP operates based on the combined solar and geothermal energy sources. A structure with two reversing valves is added to allow heating in winter (heating mode) and cooling in summer (cooling mode).
- Higher condenser and evaporator temperatures negatively and positively influence COP, respectively. Optimal generator temperature leads to the best performance of the system.
- A multiobjective optimization was conducted and the result shows that an increase in the COP would decrease the NPV. The optimal design solutions are listed and need to be selected.
- The exergy loss mainly occurs in the solar collector and thermal energy storage, followed by the heat exchangers.

Data Availability Statement

All data, models, and code generated or used during the study appeared in the published article.

Acknowledgments

The authors gratefully acknowledge the financial support by the National Key Research and Development Program of China (Grant No. 2017YFB0603500) and the National Natural Science Foundation of China (Grant No. 51976147). Z.E.L. and K.M.Z. are supported by the National Science Foundation (NSF) under Grant No. 1711546.

Notation

The following symbols are used in this paper:

- C = cost (¥), concentration ratio;
- E = exergy (kW);
- h = specific enthalpy (kJ/kg);
- I = exergy loss rate (kW), radiation (W/m^2);
- L = length (m);
- \dot{m} = mass flow rate (kg/s);
- Q = heat load (kW);
- R = tilt factor for radiation;
- r = discount factor;
- S = incident solar flux (W/m^2);
- s = specific entropy (kJ/kg·K);
- T = temperature (K);

- U = heat transfer coefficient ($\text{W}/\text{m}^2\cdot\text{K}$);
- V = volume (m^3);
- x = concentration;
- α = absorptivity;
- η = efficiency;
- ρ = reflectivity, density (kg/m^3); and
- τ = transmissivity.

Subscripts

- abso = absorb;
- ahp = absorption heat pump;
- amb = ambient;
- bm = beam;
- cond = condenser;
- dif = diffuse;
- evap = evaporator;
- gene = generator;
- gh = ground source heat exchanger;
- hc s = high-concentration stream;
- HEX = heat exchanger;
- lcs = low-concentration stream;
- ref = reference; and
- stg = storage.

References

- Banat, F., and N. Jwaied. 2008. "Exergy analysis of desalination by solar-powered membrane distillation units." *Desalination* 230 (1–3): 27–40. <https://doi.org/10.1016/j.desal.2007.11.013>.
- Bellos, E., and C. Tzivanidis. 2019. "Multi-objective optimization of a solar assisted heat pump-driven by hybrid PV." *Appl. Therm. Eng.* 149 (Feb): 528–535. <https://doi.org/10.1016/j.applthermaleng.2018.12.059>.
- Braimakis, K., A. Thimo, and S. Karellas. 2017. "Technoeconomic analysis and comparison of a solar-based biomass ORC-VCC system and a PV heat pump for domestic trigeneration." *J. Energy Eng.* 143 (2): 04016048. [https://doi.org/10.1061/\(ASCE\)EY.1943-7897.0000397](https://doi.org/10.1061/(ASCE)EY.1943-7897.0000397).
- Chua, K. J., S. K. Chou, and W. M. Yang. 2010. "Advances in heat pump systems: A review." *Appl. Energy* 87 (12): 3611–3624. <https://doi.org/10.1016/j.apenergy.2010.06.014>.
- El-Gohary, M. M. 2013. "Economic analysis of combined fuel cell generators and absorption chillers." *Alexandria Eng. J.* 52 (2): 151–158. <https://doi.org/10.1016/j.aej.2012.12.004>.
- Hawladar, M. N. A., S. K. Chou, and M. Z. Ullah. 2001. "The performance of a solar assisted heat pump water heating system." *Appl. Therm. Eng.* 21 (10): 1049–1065. [https://doi.org/10.1016/S1359-4311\(00\)00105-8](https://doi.org/10.1016/S1359-4311(00)00105-8).
- Hernández-Magallanes, J. A., C. L. Heard, R. Best, and W. Rivera. 2018. "Modeling of a new absorption heat pump-transformer used to produce heat and power simultaneously." *Energy* 165 (Part A): 112–133. <https://doi.org/10.1016/j.energy.2018.09.074>.
- IEA (International Energy Agency). 2017. *District energy systems in China: Options for optimisation and diversification*. Paris: IEA.
- Ji, J., G. Pei, T. Chow, K. Liu, H. He, J. Lu, and C. Han. 2008. "Experimental study of photovoltaic solar assisted heat pump system." *Sol. Energy* 82 (1): 43–52. <https://doi.org/10.1016/j.solener.2007.04.006>.
- Jia, T., and Y. Dai. 2018. "Development of a novel unbalanced ammonia-water absorption-resorption heat pump cycle for space heating." *Energy* 161 (Oct): 251–265. <https://doi.org/10.1016/j.energy.2018.07.128>.
- Kuang, Y. H., and R. Z. Wang. 2006. "Performance of a multi-functional direct-expansion solar assisted heat pump system." *Sol. Energy* 80 (7): 795–803. <https://doi.org/10.1016/j.solener.2005.06.003>.
- Lior, N., and N. Zhang. 2007. "Energy, exergy, and second law performance criteria." *Energy* 32 (4): 281–296. <https://doi.org/10.1016/j.energy.2006.01.019>.

- Lukawski, M. Z., B. J. Anderson, C. Augustine, L. W. Capuano, K. F. Beckers, B. Livesay, and J. W. Tester. 2014. "Cost analysis of oil, gas, and geothermal well drilling." *J. Pet. Sci. Eng.* 118 (Jun): 1–14. <https://doi.org/10.1016/j.petrol.2014.03.012>.
- Mazzeo, D. 2019. "Solar and wind assisted heat pump to meet the building air conditioning and electric energy demand in the presence of an electric vehicle charging station and battery storage." *J. Cleaner Prod.* 213 (Mar): 1228–1250. <https://doi.org/10.1016/j.jclepro.2018.12.212>.
- Mroz, T. M. 2006. "Thermodynamic and economic performance of the LiBr–H₂O single stage absorption water chiller." *Appl. Therm. Eng.* 26 (17–18): 2103–2109. <https://doi.org/10.1016/j.applthermaleng.2006.04.013>.
- NIST. 2013. *NIST thermodynamic and transport properties of refrigerants and refrigerant mixtures REFPROP, Version 9.1*. Gaithersburg, MD: NIST.
- Ozgener, O. 2010. "Use of solar assisted geothermal heat pump and small wind turbine systems for heating agricultural and residential buildings." *Energy* 35 (1): 262–268. <https://doi.org/10.1016/j.energy.2009.09.018>.
- Ozgener, O., and A. Hepbasli. 2005. "Performance analysis of a solar-assisted ground-source heat pump system for greenhouse heating: An experimental study." *Build. Environ.* 40 (8): 1040–1050. <https://doi.org/10.1016/j.buildenv.2004.08.030>.
- Song, Y., M. Zou, J. Deng, and X. Chen. 2019. "Case study on passive heat compensation tower of ground-source heat-pump system." *J. Energy Eng.* 145 (6): 05019002. [https://doi.org/10.1061/\(ASCE\)EY.1943-7897.0000629](https://doi.org/10.1061/(ASCE)EY.1943-7897.0000629).
- Sukhatme, S. P. 1984. *Solar energy principles of thermal collection and storage*. New Delhi, India: McGraw-Hill.
- Thygesen, R., and B. Karlsson. 2014. "Simulation and analysis of a solar assisted heat pump system with two different storage types for high levels of PV electricity self-consumption." *Sol. Energy* 103 (May): 19–27. <https://doi.org/10.1016/j.solener.2014.02.013>.
- Tsoutsos, T., J. Anagnostou, C. Pritchard, M. Karagiorgas, and D. Agoris. 2003. "Solar cooling technologies in Greece. An economic viability analysis." *Appl. Therm. Eng.* 23 (11): 1427–1439. [https://doi.org/10.1016/S1359-4311\(03\)00089-9](https://doi.org/10.1016/S1359-4311(03)00089-9).
- Udayakumar, M. 2008. "Studies of compressor pressure ratio effect on GAXAC (generator–absorber–exchange absorption compression) cooler." *Appl. Energy* 85 (12): 1163–1172. <https://doi.org/10.1016/j.apenergy.2008.03.002>.
- Ünal, F., G. Temir, and H. Köten. 2018. "Energy, exergy and exergoeconomic analysis of solar-assisted vertical ground source heat pump system for heating season." *J. Mech. Sci. Technol.* 32 (8): 3929–3942. <https://doi.org/10.1007/s12206-018-0744-1>.
- Voros, N. G., C. T. Kiranoudis, and Z. B. Maroulis. 1998. "Solar energy exploitation for reverse osmosis desalination plants." *Desalination* 115 (1): 83–101. [https://doi.org/10.1016/S0011-9164\(98\)00029-0](https://doi.org/10.1016/S0011-9164(98)00029-0).
- Wu, W., S. Ran, W. Shi, B. Wang, and X. Li. 2016. "NH₃-H₂O water source absorption heat pump (WSAHP) for low temperature heating: Experimental investigation on the off-design performance." *Energy* 115 (Part 1): 697–710. <https://doi.org/10.1016/j.energy.2016.09.058>.
- Wu, W., B. Wang, W. Shi, and X. Li. 2014a. "Absorption heating technologies: A review and perspective." *Appl. Energy* 130 (Oct): 51–71. <https://doi.org/10.1016/j.apenergy.2014.05.027>.
- Wu, W., T. You, B. Wang, W. Shi, and X. Li. 2014b. "Simulation of a combined heating, cooling and domestic hot water system based on ground source absorption heat pump." *Appl. Energy* 126 (Aug): 113–122. <https://doi.org/10.1016/j.apenergy.2014.04.006>.
- Wu, Z., S. You, H. Zhang, and M. Fan. 2019. "Mathematical modeling and performance analysis of seawater heat exchanger in closed-loop seawater-source heat pump system." *J. Energy Eng.* 145 (4): 04019012. [https://doi.org/10.1061/\(ASCE\)EY.1943-7897.0000608](https://doi.org/10.1061/(ASCE)EY.1943-7897.0000608).
- Zhang, X., and K. M. Zhang. 2015. "Demand response, behind-the-meter generation and air quality." *Environ. Sci. Technol.* 49 (3): 1260–1267. <https://doi.org/10.1021/es505007m>.
- Zheng, W., T. Ye, S. You, and H. Zhang. 2016a. "Experimental investigation of the heat transfer characteristics of a helical coil heat exchanger for a seawater-source heat pump." *J. Energy Eng.* 142 (1): 04015013. [https://doi.org/10.1061/\(ASCE\)EY.1943-7897.0000272](https://doi.org/10.1061/(ASCE)EY.1943-7897.0000272).
- Zheng, Z., Y. Xu, J. Dong, and L. Zhang. 2016b. "Design and experimental testing of a ground source heat pump system based on energy-saving solar collector." *J. Energy Eng.* 142 (3): 04015022. [https://doi.org/10.1061/\(ASCE\)EY.1943-7897.0000288](https://doi.org/10.1061/(ASCE)EY.1943-7897.0000288).